A Climatology of Midlatitude Mesoscale Convective Vortices in the Rapid Update Cycle

ERIC P. JAMES AND RICHARD H. JOHNSON

Department of Atmospheric Science, Colorado State University, Fort Collins, Colorado

(Manuscript received 31 August 2009, in final form 25 November 2009)

ABSTRACT

Climatological characteristics of mesoscale convective vortices (MCVs) occurring in the state of Oklahoma during the late spring and summer of four years are investigated. The MCV cases are selected based on vortex detection by an objective algorithm operating on analyses from the Rapid Update Cycle (RUC) model. Consistent with a previous study, true MCVs represent only about 20% of the mesoscale relative vorticity maxima detected by the algorithm. The MCVs have a broad range of radii and intensities, and their longevities range between 1 and 54 h. Their median radius is about 200 km, and their median midlevel relative vorticity is 1.2×10^{-4} s^{-1}. There appears to be no significant relationship between MCV longevity and intensity. Similar to past estimates, approximately 40% of the MCVs generate secondary convection within their circulations.

The mean synoptic-scale MCV environment is determined by the use of a RUC-based composite analysis at four different stages in the MCV life cycle, defined based on vortex detection by the objective algorithm. MCV initiation is closely tied to the diurnal cycle of convection over the Great Plains, with MCVs typically forming in the early morning, near the time of maximum extent of nocturnal mesoscale convective systems (MCSs). Features related to the parent MCSs, including upper-level divergent outflow, midlevel convergence, and a low-level jet, are prominent in the initiating MCV composite. The most significant feature later in the MCV life cycle is a persistent mesoscale trough in the midlevel height field. The potential vorticity (PV) structure of the composite MCV consists of a midlevel maximum and an upper-level minimum, with some extension of elevated PV into the lower troposphere as the vortex matures. The environment immediately downshear of the MCV is more conducive to secondary convection than the environment upshear of the MCV.

This midlatitude MCV climatology represents an extension of past individual case studies by providing mean characteristics of a large MCV population; these statistics are suitable for the verification of MCV simulations. Also presented is the first high-resolution composite analysis of the MCV environment at different stages of the MCV life cycle, which will aid in identifying and forecasting these systems.

1. Introduction

Mesoscale convective vortices (MCVs) have become a topic of increasing interest in mesoscale meteorology over the past 30 years, largely due to the recognition of their influence on the initiation, organization, and evolution of deep, moist convection. These vortices are quasi-steady, mesoscale, cyclonic circulations that form in the midtroposphere within the stratiform regions of mesoscale convective systems (MCSs), often persisting after the dissipation of the parent MCS. MCVs are sometimes responsible for the repeated generation of convection in so-called serial MCSs (Bosart and Sanders 1981; Fritsch et al. 1994), play a role in organizing convection within extreme-rain-producing MCSs (Trier and Davis 2002; Schumacher and Johnson 2008, 2009), and have been implicated in some cases of tropical cyclogenesis (Velasco and Fritsch 1987). Additional research on the structure and climatology of MCVs is needed to improve our understanding and forecasting of these associated hazards.

Numerous studies have described the climatological characteristics of MCSs in the central United States. It has been shown that there is a diurnal signal in MCS frequency in this region during the warm season, with afternoon convection on the east slopes of the Rocky Mountains developing into eastward-propagating MCSs during the night (Carbone et al. 2002). Similar propagating signals have recently been found in tropical regions of frequent MCS activity (e.g., Wang et al. 2005;

Corresponding author address: Eric James, Dept. of Atmospheric Science, Colorado State University, 1371 Campus Delivery, Fort Collins, CO 80523-1371.
E-mail: ejames@atmos.colostate.edu

DOI: 10.1175/2009MWR3208.1

Laing et al. 2008; Keenan and Carbone 2008). A subset of MCSs, mesoscale convective complexes (MCCs; Maddox 1980), has been extensively studied both in the United States and abroad (e.g., Cotton et al. 1983; Wetzel et al. 1983; Velasco and Fritsch 1987; Miller and Fritsch 1991; Laing and Fritsch 1993a,b). Composite analyses have revealed key features in the environment of MCCs, including a low-level jet (LLJ) and associated warm advection, a midlevel shortwave trough, and upper-level divergent outflow (Maddox 1983; Cotton et al. 1989). There are some indications that MCVs are another fundamental feature of MCCs, causing their quasi-circular shape and contributing to their longevity (Velasco and Fritsch 1987; Olsson and Cotton 1997). In addition, MCVs are present in many MCSs that do not meet the stringent MCC size and duration criteria of Maddox (1980). If MCVs do indeed exist in most MCCs and MCSs, common features should emerge from composite analyses of these interrelated systems.

Past studies addressing the climatological characteristics of MCVs have used various methods to select and analyze cases in the United States. Early work by Bartels and Maddox (1991, hereafter BM) focused on the synoptic environments of MCVs. Their subjective detection method involved searching 4-km visible satellite imagery for systems that exhibit well-defined cloud bands for more than 1 h and whose ''shape and pattern suggest cyclonic rotation, even when viewed on a single satellite image.'' This method, applied to approximately 8 yr of satellite imagery over the central United States, appears to significantly underestimate the total number of MCVs occurring. This is likely due to the limitations of the satellite imagery; MCVs are only detected if they have well-defined cyclonic curvature in the low- and midlevel clouds, with limited view-obstructing upper-level cirrus. BM found 24 events, and determined that MCVs are favored in situations with weak flow, weak vertical wind shear, weak background relative vorticity, and intense vertical and horizontal moisture gradients.

A more recent study by Trier et al. (2000, hereafter TDT) used a larger variety of observations in their MCV detection, including radar reflectivity, infrared satellite imagery, and National Oceanic and Atmospheric Administration (NOAA) Profiler Network (NPN) wind profiles. They considered an MCV to exist whenever a circulation was indicated by any of these platforms after the dissipation of convection associated with the parent MCS. Using this method, TDT detected 16 MCVs during the convective season of 1998. They found that, on average, MCVs occur in environments with weaker shear than the environments of the general MCS population. Regeneration of convection occurred in slightly more than half of their MCV cases.

Davis et al. (2002, hereafter DAT) investigated MCV detection and prediction by the Rapid Update Cycle (RUC; Benjamin et al. 2004) model. They developed an automated algorithm that is capable of distinguishing MCVs from synoptic-scale vorticity features in RUC analyses, and demonstrated its ability to detect MCVs over the Great Plains during the convective season of 1999. It was found that true MCVs constitute fewer than half of the midlevel mesoscale vortices appearing in the RUC during the season of interest. The RUC appears to be devoid of skill in predicting MCV development in advance, due to shortcomings in its forecasts of MCS activity.

This paper extends the work of DAT by applying their algorithm to four additional years, allowing comparison with their results. We also present a composite analysis of the synoptic-scale environment of the MCVs at different points in the life cycle. Our main goal is to provide a broad climatological overview of the frequency, structure, and environment of midlatitude MCVs based on consistent, high-resolution RUC analyses. It is hoped that such a climatology will facilitate generalizations about the physical characteristics of MCVs, which will help to synthesize and solidify the conclusions reached in the large number of individual MCV case studies that have been carried out. It is also anticipated that the large population of MCVs investigated herein will provide a statistically robust basis for the validation of numerical simulations of MCVs, from both the numerical weather prediction (NWP) and general circulation modeling (GCM) perspectives. The remainder of this paper is organized as follows. The methodology used for selecting MCV cases and constructing a composite MCV is described in section 2. Section 3 summarizes the frequency and structure of the detected MCVs. The composite analysis is presented in section 4. A summary and some conclusions are offered in section 5.

2. Methodology

The details of the MCV detection algorithm are provided by DAT and modifications to the algorithm for the purposes of the present study are described by James and Johnson (2010). DAT used their algorithm to search for MCVs throughout the central United States (see their Fig. 1); in this study, we apply the algorithm only over a latitude–longitude box containing the state of Oklahoma (33.5°–37°N, 94.5°–103°W). Our domain is limited to Oklahoma because of the presence of the Oklahoma Mesonet, which was used to analyze the surface features of the MCVs (James and Johnson 2010). DAT ran the algorithm on 3-h RUC analyses; we use hourly analyses. We analyze the same season as DAT,

the months of May–August, over the years 2002–05. The version of the RUC in use during these years has a horizontal grid spacing of 40 km, and the data are archived at vertical levels every 25 hPa. The algorithm produces hourly maps of grid points satisfying several objective vortex criteria (including minimum ''roundness'' and maximum size thresholds). Detected vortices, which can be followed from hour to hour, are considered to be MCVs only if they are embedded within, or arise from, significant stratiform precipitation and anvil cloud associated with deep, moist convection. Fifteen-minute composite radar reflectivity imagery is used to identify regions of convective and stratiform precipitation. Unlike DAT, we do not require a specific level of temporal continuity in the algorithm's MCV detections. As long as an MCV can be continuously followed in the radar or satellite imagery, we consider multiple, temporally distinct, periods of detection by the algorithm to be a single MCV. The number of our detected vortices is limited by the extensive periods of missing RUC data during two of the four study years; the 2002 data are 39% complete, and the 2005 data are 38% complete. The other two years have greater than 85% data coverage.

To examine MCV life cycles, it is necessary to determine the life cycle evolution of each case. Ideally, pure observations could be used to track the intensity of each vortex, and some objective criteria could be used to define life cycle stages; however, upper-air observations are too sparse to allow this. To circumvent this issue, we utilize the RUC model to follow the evolution of the MCVs throughout their life cycles. Four life cycle stages are defined based on the timing of the vortex detection by the objective algorithm.

MCV initiation is defined as the hour at which an MCV is first detected by the objective algorithm. MCV maturity is defined as the hour at which the MCV attains its maximum relative vorticity at any level between 600 and 500 hPa. MCV dissipation is defined as the hour at which the MCV is last detected by the objective algorithm. Finally, MCV development is defined as the analysis hour that is halfway between initiation and maturity (rounded up). While these stages of the life cycle of an MCV are admittedly arbitrary, they are at least consistent among all cases, and should be expected to provide a basic sense of the evolution of different MCVs. The RUC certainly has deficiencies in its representation of MCVs; however, the advantage of using the RUC is its consistency among all times, allowing an objective comparison of the longevity and evolution of different cases.

We construct synoptic-scale composites of each of these four life cycle stages based on the RUC analyses. Each MCV case with valid RUC data at the times of interest is included in these composites. The RUC analysis grids are shifted such that the composite vortex is centered at the mean MCV location at each life cycle stage. The shifting of the grids is based on the position of the 600–500-hPa relative vorticity maximum associated with each MCV at each analysis time. Due to the coarse resolution of the RUC data, these composites are mainly of use for investigating the synoptic-scale environment of MCVs at different stages of their life cycles.

TABLE 1. Comparison of the number of MCVs found in previous studies with this study. Numbers in parentheses indicate the total numbers of vortices (including non-MCVs) detected by the objective algorithm of DAT.

Study	Time period	Number of MCVs
BM	1 Jan 1981–30 Sep 1988	24
TDT	15 May–15 Sep 1998	16
DAT	1 May–31 Aug 1999	43 (203)
This study	1 May–31 Aug 2002	20 (113)
This study	1 May–31 Aug 2003	21 (134)
This study	1 May–31 Aug 2004	39 (136)
This study	1 May–31 Aug 2005	15 (59)

3. MCV climatology

In this section, we present our main findings concerning the frequency and structure of the midlatitude MCVs that are detected by the objective algorithm of DAT during the convective seasons of 2002–05. Many of the MCV properties described here can be directly compared with those found by DAT during the convective season of 1999.

a. Frequency

The results of the MCV detection algorithm over the study periods of May–August 2002–05 are presented and compared with previous MCV climatologies in Table 1. The previous climatologies have been summarized in section 1; it should be noted that their detection methodologies have been of variable sophistication and efficiency. It is also important to recognize the differences in the experimental design between this study and that of DAT, despite the use of the same algorithm. DAT ran the algorithm on 3-hourly RUC analyses, whereas hourly analyses are used in this study. Additionally, DAT documented vortices throughout the Great Plains, whereas this study focuses on vortices only in the vicinity of Oklahoma.

This study finds 95 MCVs over the 4 yr of interest, with between 15 and 39 occurring each year. This is a significantly larger annual frequency of MCVs than has been found by BM or TDT, even though those earlier studies covered a much broader area. This frequency difference likely occurs because neither BM nor TDT counted

MCVs unless the parent MCS had dissipated, whereas we include many short-lived MCVs within active MCSs. Keeping in mind the large number of missing RUC analyses in 2002 and 2005, we can estimate that, in an average year, approximately 30 MCVs occur over Oklahoma and the Texas Panhandle, out of perhaps $\sim 10^2$ throughout the Great Plains. The numbers in parentheses in Table 1 indicate the total numbers of vortices (i.e., the sum of MCVs and non-MCV vortices) for each year. Interestingly, both in this study and in DAT, the non-MCV vortices detected by the algorithm outnumber the actual MCVs. The differences in the domain sizes, the temporal resolution of the RUC analyses, and the extent of the missing data in the two studies can be overcome by comparing percentages of vortices that are MCVs. MCVs account for 21% of the vortices detected by the objective algorithm in this study; the percentage found by DAT was also 21%. Given the design of the algorithm, and within its inherent limitations, we can conclude that MCVs constitute about 20% of the mesoscale, circular, midlevel summertime vortices occurring in the Great Plains.

In the remainder of this paper, we focus only on those MCVs that move over the main part of Oklahoma at some point during their life cycle; this subset comprises 45 of the 95 MCV events. These MCV cases are the same as those analyzed by James and Johnson (2010) and are listed in the appendix to that article.

For the MCV cases having valid RUC analyses at their initiation and dissipation, it is possible to determine the vortex longevity. This is defined as the number of hourly RUC analyses between the initiation and dissipation of a single MCV, including the initiation and dissipation hours. The distribution of MCV longevity is shown in Fig. 1. The distribution is quite asymmetric, with a long tail toward longer MCV lifetimes; the longest-lived MCV in this study, occurring during 29 June–1 July 2003, lasts for 54 h. The peak in the longevity of the cases examined is 6–10 h. Four cases last 5 h or less. It should be noted that, although some of the MCVs included here spend only a brief time over Oklahoma, it is possible to track the vortices before and after their passage of Oklahoma using the RUC analyses, which cover the entire contiguous United States.

Further insight into the evolution of the MCVs is obtained by examining the timing of the stages of the life cycle with respect to the diurnal cycle. Figure 2 shows a histogram of the hour of MCV initiation, in local time (LT; UTC − 6 h). There is a clear preference for MCV initiation to occur in the early morning hours, between 2300 and 0700 LT. Interestingly, this time period corresponds to the time of maximum areal extent in studies of central U.S. MCCs. Thirty-two of the 43 MCCs identified by Maddox (1980) during 1978, and 9 of the

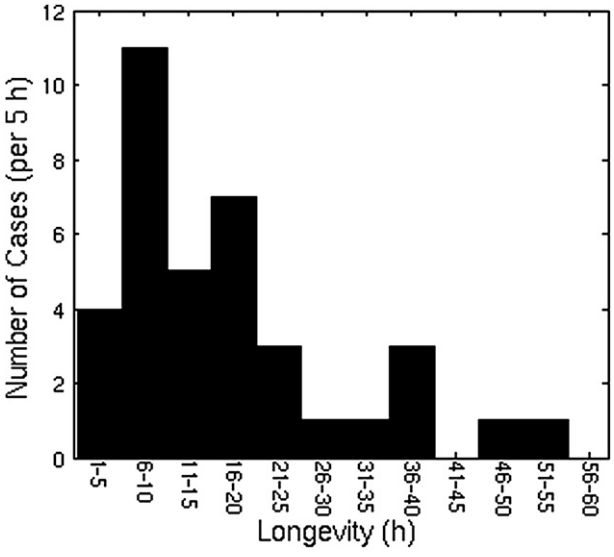

FIG. 1. Histogram of MCV longevity, defined as the number of hours an MCV is detected by an objective algorithm.

10 MCCs included in the composite of Maddox (1983), reached their maximum extent during this period of the day. This is strong evidence for the close association of MCCs and MCVs; MCVs tend to form toward the end of the life cycle of nocturnal MCCs (Velasco and Fritsch 1987). There are very few MCV initiations between 1300 and 2300 LT, demonstrating that MCV initiation is quite strongly tied to the diurnal cycle. The reason for the secondary peak in initiation near local noon is not clear.

Figures 3 and 4 show similar histograms of the timing of maturity and dissipation, respectively, among the MCV cases with respect to the diurnal cycle. The timing of these stages of the life cycle appears increasingly independent of the diurnal cycle, with maturity showing a slight preference for late morning (0600–1200 LT) and dissipation showing no significant peak at any time of day. Taken together, these results suggest that MCVs follow a diurnal cycle in their evolution only to the extent that they initiate within nocturnal MCSs. It appears that, once formed, MCVs are largely independent of the diurnal cycle, with their longevity being determined by the environmental conditions (TDT). However, the reinvigoration of MCVs by their secondary convection (a second cycle of deep convective activity during the MCV lifetime) may be tied to the diurnal cycle (Fritsch et al. 1994; Trier and Davis 2002). It should be noted that the timing of the MCV life cycle stages presented here depends on the successful capture of the MCVs by the RUC analyses. As pointed out by DAT, there is likely a bias toward MCV detection at synoptic times (i.e., 0000, 0600, 1200, and 1800 UTC), although this bias is reduced by the assimilation of hourly NPN wind profiles into the RUC.

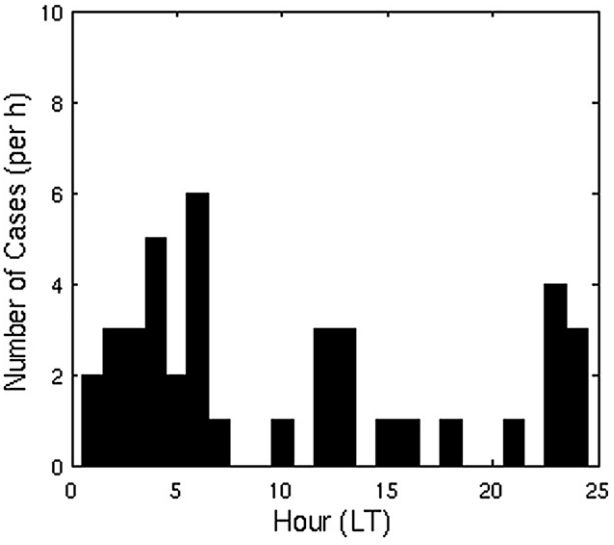

FIG. 2. Histogram of the diurnal timing of MCV initiation (LT).

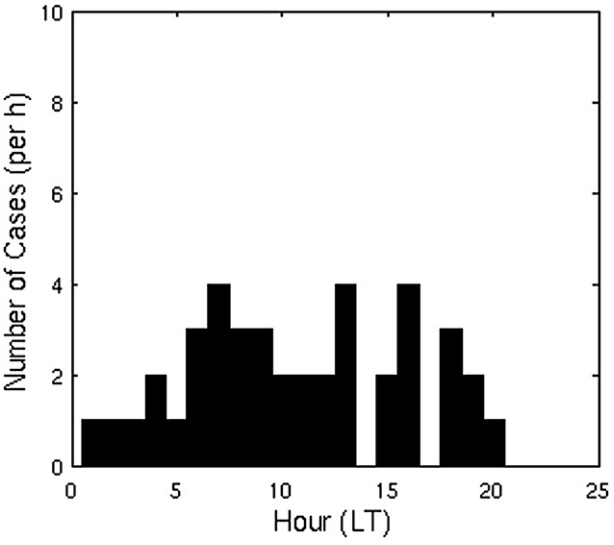

FIG. 3. Histogram of the diurnal timing of MCV maturity (LT).

b. Structure

Figure 5 displays the distribution of MCV sizes documented in this study. The MCV radius R is the same as that defined by DAT; it is the radius bin of RUC grid points at which the azimuthally averaged 600–500-hPa relative vorticity first falls below 10% of the MCV's maximum (central) relative vorticity. Figure 5 can be compared with Fig. 8 in DAT; the metric is equivalent. However, DAT include vortices arising from non-MCS convection in their Fig. 8. In their larger sample of MCV cases, taken from the entire Great Plains, DAT found a median vortex radius in bin 5, corresponding to an average radius of 185 km; the median radius in this study is located in bin 6, corresponding to an average radius of 224 km. It is not known if this is a real difference between the years 1999 and 2002–05, a result of the different regions covered in the two studies, or a statistical artifact. Both studies demonstrate that the median MCV radius is below bin 7 (262 km), indicating that the cutoff radius of 300 km used in the MCV detection algorithm (DAT) is likely appropriate.

The distribution of intensity of the MCV cases is shown in Fig. 6. For the purposes of this study, MCV intensity is defined as the mean 600–500-hPa relative vorticity at system maturity. MCV intensity varies between 2×10^{-5} and 2.3×10^{-4} s^{-1}, with a broad peak between 9×10^{-5} and 1.4×10^{-4} s^{-1}. This distribution of the MCV relative vorticity agrees quite well with that found by DAT (displayed in their Fig. 9c). The exact relative vorticity values are likely somewhat dependent upon the model resolution.

In addition to the metrics described thus far, DAT determined the frequency of MCVs that trigger secondary convection. Their definition of secondary convection, used again in this study, is the appearance of new radar echoes of greater than 40-dBZ reflectivity within 200 km of the MCV center. They found that 20 of their 43 MCV cases, or 46%, had convective retriggering. TDT found that 9 of their 16 cases, or 56%, generated secondary convection. In this study, 17 of the 45 cases, or 38%, generate secondary convection within their circulations. The MCVs with secondary convection have a median longevity in the range of 16–20 h (not shown), with much shorter- and longer-lived cases also sometimes occurring. The mean longevity of MCVs with secondary convection, however, is not significantly different from that of the entire MCV sample.

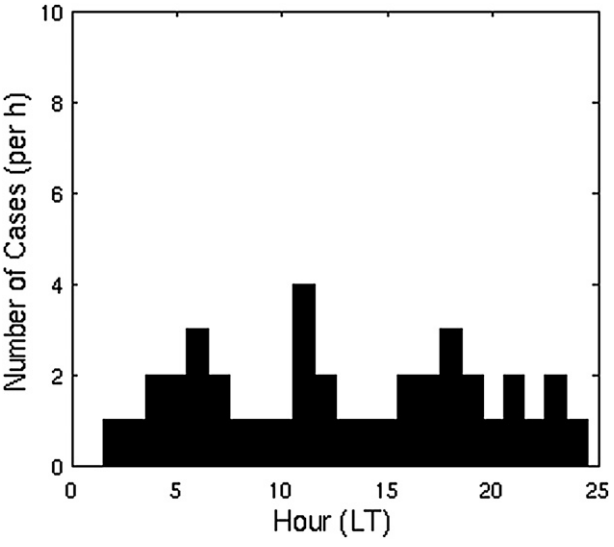

FIG. 4. Histogram of the diurnal timing of MCV dissipation (LT).

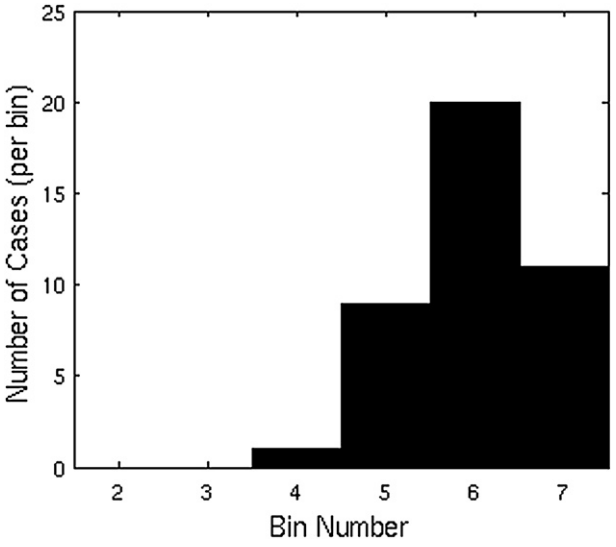

FIG. 5. Histogram of the MCV radius at system maturity, defined as the radius bin at which the MCV's azimuthally averaged 600–500-hPa relative vorticity first falls below 10% of the central (maximum) relative vorticity. Bins 2–7 correspond to average radii of 49, 97, 142, 185, 224, and 262 km, respectively.

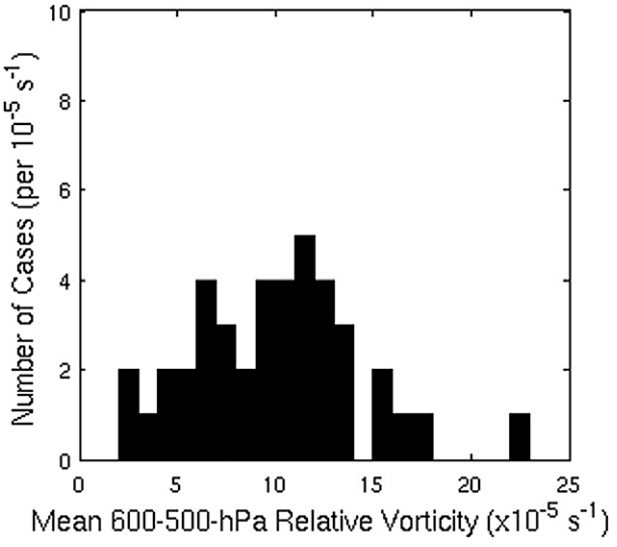

FIG. 6. Histogram of MCV intensity, defined as the central 600–500-hPa average relative vorticity at system maturity (10^{-5} s^{-1}).

Figure 7 shows a scatterplot of the natural logarithm of MCV longevity versus the natural logarithm of intensity; this plot reveals that there is essentially no relationship between these variables. The scatterplot is presented in logarithmic form to facilitate comparison with Fig. 11 of DAT. Figure 11 in DAT includes dry vortices, many of which are weak and short lived; dry vortices are excluded from our analysis. Thus, comparison should be made with the distribution of only ''MCS''-type vortices in Fig. 11 of DAT. DAT found a distinct lack of weak, long-lived vortices, but this type of MCV does occur in our sample. This could be due to their requirement, relaxed in this study, that MCVs be nearly continuously detected by the RUC algorithm. Weaker MCVs, with ill-defined circulations in the upper-air observations (and therefore the RUC), are likely to be only intermittently detected by the automated algorithm, even though they can be continuously followed in satellite or radar imagery. This would lead to a low bias in DAT's MCV longevity. This suggests that their lack of weak, long-lived MCVs could be artificial.

4. Composite MCV

This section presents the results of the composite analysis at the four different MCV life cycle stages defined in section 2. We describe the motion of the composite vortex, summarize its synoptic-scale environment, and examine the influences of vertical wind shear superimposed on the MCV. The initiation, development, maturity, and dissipation composites omit 5, 7, 6, and 6 of the 45 MCV cases, respectively, due to missing RUC data at the appropriate analysis times.

a. Vortex motion

Averaged over its life cycle, the composite MCV moves east-southeastward at 7 m s^{-1}. The vortex motion slows slightly and veers later in the life cycle. To search for a possible ''steering level'' for the composite

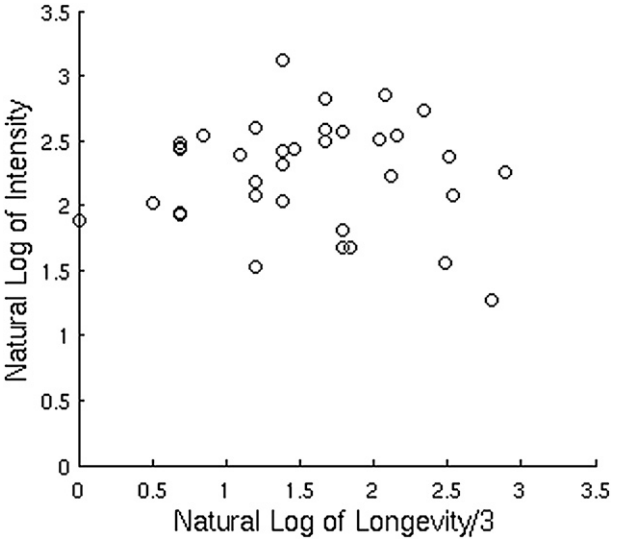

FIG. 7. Scatterplot of ln(MCV longevity) vs ln(intensity; defined as the central 600–500-hPa average relative vorticity at system maturity; 10^{-5} s^{-1}). Longevity has been divided by three, and intensity has been scaled by 10^5, before applying the natural log operator. Compare with Fig. 11 of Davis et al. (2002).

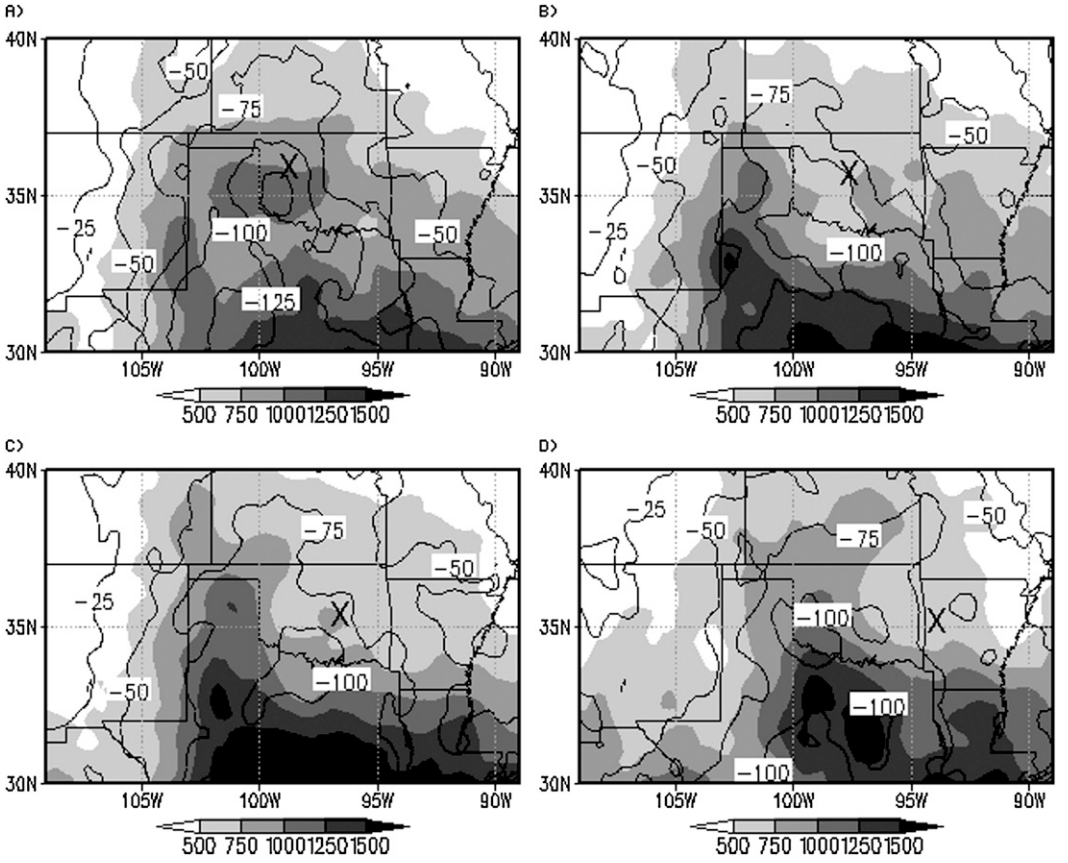

FIG. 8. RUC analyses of surface-based CAPE (J kg^{-1}; shaded, with scale at bottom) and CIN [J kg^{-1}; contour interval (CI) 25 J kg^{-1}] at the (a) initiation, (b) development, (c) maturity, and (d) dissipation stages of the composite MCV. Composite vortex center is marked by a large cross in (a)–(d).

MCV, we examine the environmental wind profile of each constituent vortex at each life cycle stage. Wind profiles are derived from the RUC; to isolate the environment of the MCV, we average the wind profiles over a 2° radius circle centered on the vortex. A single wind profile is then calculated for each MCV case by averaging the profiles over the four life cycle stages. We then compute the correlation coefficients between MCV motion and the wind at each height among all the cases. Using this method, we find that the maximum correlation between the vortex heading and the environmental wind direction occurs at 550 hPa ($r^2 = 0.83$). The maximum correlation between vortex speed and environmental wind speed occurs at 500 hPa ($r^2 = 0.54$). These results are not surprising and demonstrate that MCVs are generally steered by the midlevel flow.

b. Surface features

Figure 8 shows the surface-based convective available potential energy (CAPE) and convective inhibition (CIN) in the vicinity of the composite vortex at the four life cycle stages. On the broad scale, it can be seen that the MCV forms within a general north–south instability gradient; locally, the vortex initiates just north of a region of enhanced instability (Fig. 8a). CIN is substantial near the MCV, with values greater than 100 J kg^{-1}. Such high values suggest that the convection associated with the parent MCS has likely past its peak intensity by the time of MCV initiation. Later in the MCV life cycle, a well-defined northward-pointing tongue of higher instability appears; the MCV itself is displaced significantly east of the axis of highest CAPE (Figs. 8b–d).

The composite precipitable water and surface mean sea level pressure fields are shown in Fig. 9. The sea level pressure field is likely affected by extrapolation to sea level over the high terrain of the Rocky Mountains, but the gross features of the analyses should still be valid. It is also important to note that the RUC is unable to resolve mesoscale pressure features, such as those discussed by James and Johnson (2010). It can be seen that, throughout the MCV life cycle, the surface pressure gradient points toward the east, between a large region

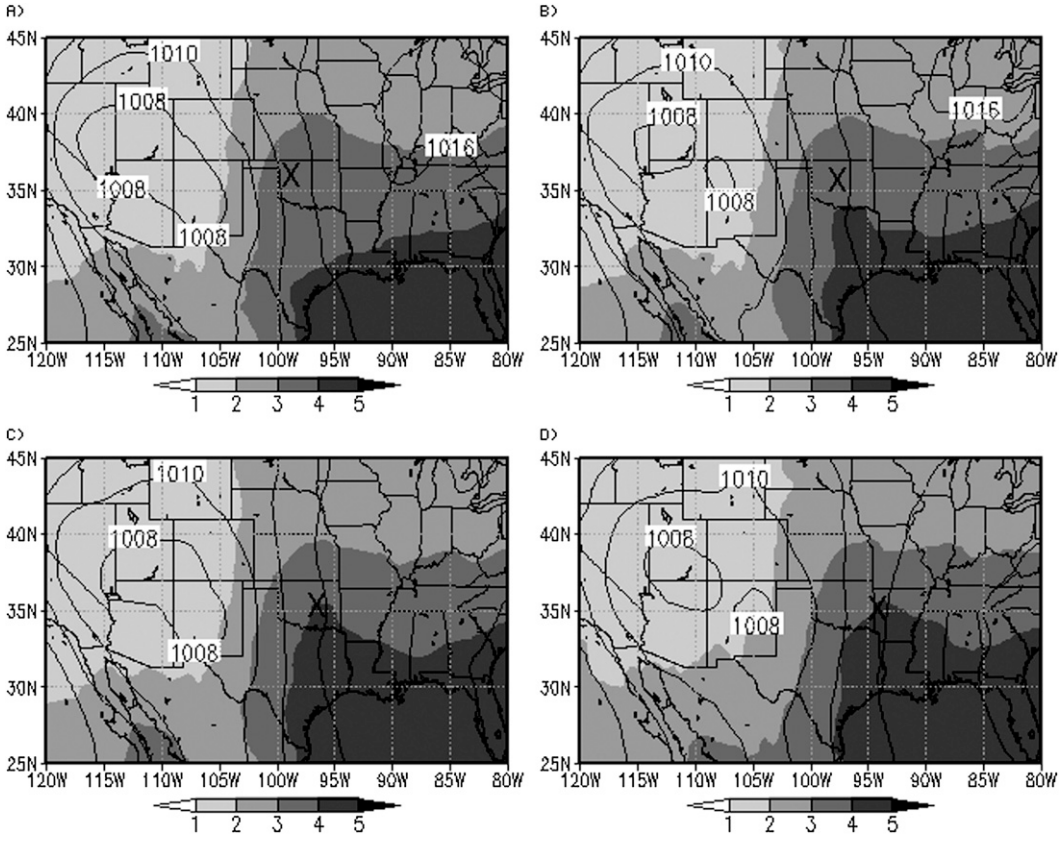

FIG. 9. RUC analyses of surface mean sea level pressure (hPa; CI 2 hPa) and column-integrated precipitable water (cm; shaded, with scale at bottom) at the (a) initiation, (b) development, (c) maturity, and (d) dissipation stages of the composite MCV. Composite vortex center is marked by a large cross in (a)–(d).

of low pressure over the higher terrain west of the MCV and the western edge of an anticyclone encroaching on the eastern United States. These pressure features resemble the climatological southwestern U.S. summertime ''heat low'' and the Atlantic Ocean ''Bermuda high.'' The pattern is similar to that typically seen during convective periods in the central Great Plains, as it allows substantial moisture return from the Gulf of Mexico on the low-level southeasterly flow. The pressure gradient appears strongest early on in the MCV life cycle (Figs. 9a and 9b). Over time, the gradient (and therefore the corresponding surface flow) in the vicinity of the MCV relaxes and veers slightly (Figs. 9c and 9d). This behavior is in agreement with the diurnal cycle of the low-level wind field over the Great Plains as simulated by Jiang et al. (2007; see their Fig. 2); the MCV initiation stage tends to occur before sunrise when winds tend to be relatively backed and strong, while the later stages of the life cycle occur throughout the diurnal cycle.

c. *Low-level features*

Figure 10 shows the composite MCV fields at the 850-hPa level. Over the central plains, this pressure level corresponds to the lower atmosphere around 1 km above the surface. However, this pressure level is below the surface over parts of the high plains and Rocky Mountains, so the fields should be viewed with caution in these locations. At MCV initiation (Fig. 10a), the height field consists of a broad trough to the northwest of the MCV, and a broad ridge to the southeast. This pattern leads to southerly or south-southwesterly winds, which correspond to the well-documented Great Plains LLJ. This low-level wind maximum is most frequently observed during the early morning hours, which is, on average, the time of MCV initiation (Fig. 2). The LLJ is also seen in the mature MCC composite of Maddox (1983; see his Fig. 5c). At this stage of the MCV life cycle, the LLJ is strongest to the southwest of the MCV, with a tongue of higher winds stretching north-northeast toward the vortex; this pattern corresponds well to the wind field seen in Fig. 5c of Maddox (1983).

During the later stages in the MCV evolution (Figs. 10b–d), the LLJ remains in a similar position with respect to the MCV, but gradually weakens. The orientation of the height contours also shifts such that the 850-hPa winds are more veered (i.e., southwesterly instead of

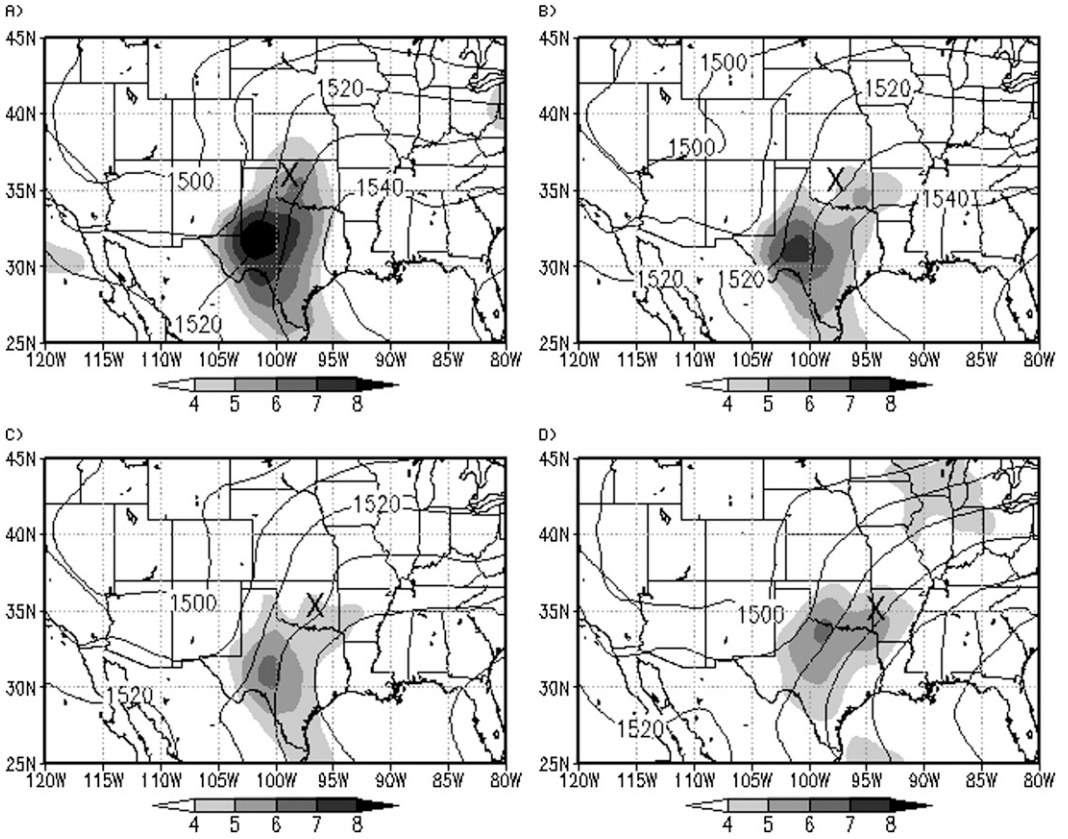

FIG. 10. RUC analyses of 850-hPa geopotential height (m; CI 10 m) and isotachs (m s^{-1}; shaded, with scale at bottom) at the (a) initiation, (b) development, (c) maturity, and (d) dissipation stages of the composite MCV. Composite vortex center is marked by a large cross in (a)–(d).

southerly). This corresponds to the average diurnal weakening and veering of the LLJ, which can also be seen in the MCC decay composite of Maddox (1983, his Fig. 6c). It is worth pointing out that, although the LLJ wind speeds are very low in the composite (below 10 m s^{-1}), this is largely a result of averaging over many MCV cases with slightly different LLJ positions. However, some MCV cases do not contain any well-defined LLJ.

Previous studies have suggested that the LLJ may often play a role in flash flood situations involving MCVs (Bosart and Sanders 1981; Davis and Trier 2002; Schumacher and Johnson 2008). The positioning of the LLJ in the southwestern quadrant of the composite MCV (Fig. 10) is consistent with the favored occurrence of extreme rainfall in this quadrant (Schumacher and Johnson 2009). The LLJ acts to rapidly transport high equivalent potential temperature air into the vicinity of the vortex; this air is then lifted, which destabilizes the environment and results in localized deep convection. Lifting mechanisms can include low-level gravity waves, density currents, or balanced lifting within the thermal structure of the MCV.

d. Midlevel features

Figure 11 shows the midlevel (500 hPa) geopotential height and relative vorticity fields at the four life cycle stages. It is apparent from Fig. 11a that the mean MCV initiation location is downstream from a midlevel ridge and upstream from a midlevel trough. This positioning agrees well with that found by BM (see their Fig. 8), despite the fewer cases identified in that study. This configuration also appears in many of the individual MCV cases included here (James and Johnson 2010). The 500-hPa relative vorticity field at MCV initiation shows weak anticyclonic relative vorticity in the environment of the MCV, particularly upstream; this is due to the anticyclonic flow around the nearby ridge. The MCV itself appears as a concentrated, circular region of cyclonic relative vorticity. At this initial time, there appears to be minimal deflection of the geopotential height contours in the vicinity of the MCV.

In the developing and mature composites (Figs. 11b and 11c), the MCV's relative vorticity intensifies to greater than 8×10^{-5} s^{-1}, while the environmental

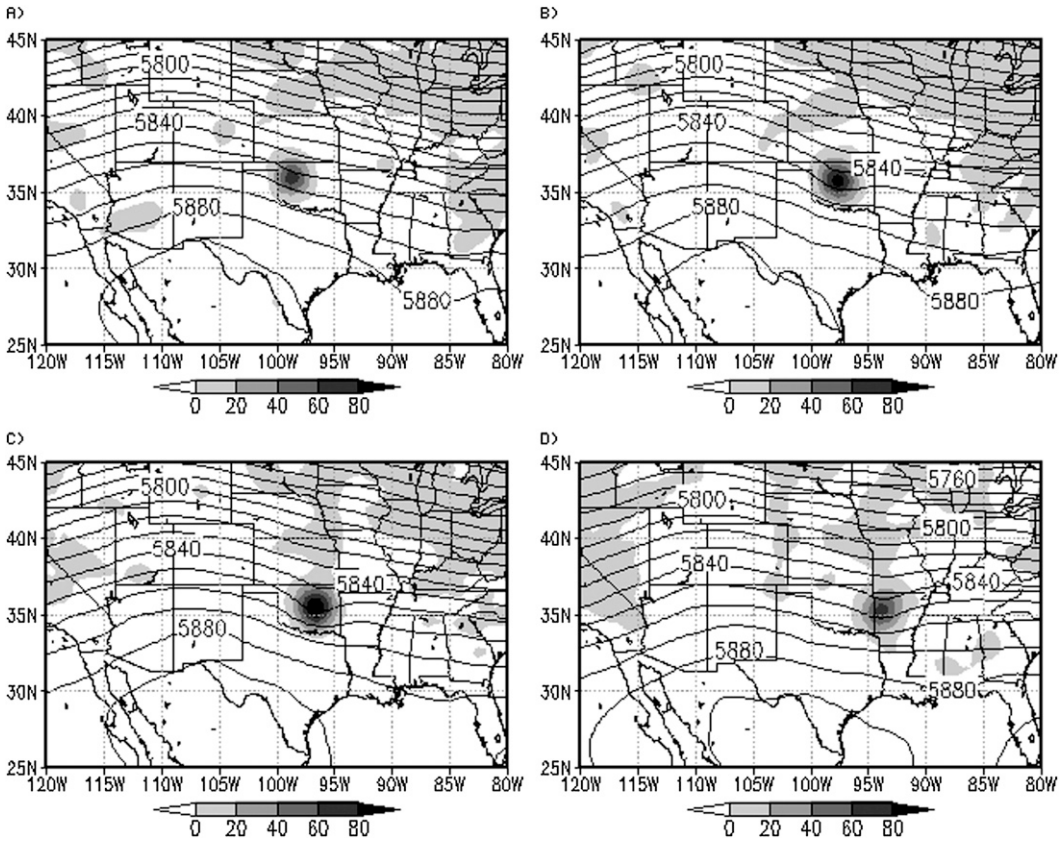

FIG. 11. RUC analyses of 500-hPa geopotential height (m; CI 10 m) and relative vorticity (10^{-6} s^{-1}; shaded, with scale at bottom) at the (a) initiation, (b) development, (c) maturity, and (d) dissipation stages of the composite MCV.

relative vorticity remains mainly anticyclonic. A pronounced mesoscale trough develops in the geopotential height field. By the time of the dissipation stage (Fig. 11d), this mesoscale trough remains very well defined, but the system's large core of cyclonic relative vorticity has weakened considerably. Maddox (1983) noted the persistence of the mesoscale trough at the trailing edge of his composite MCC (see his Fig. 6e); he remarked that this trough often becomes visible as a comma cloud in satellite imagery. This comma cloud is a manifestation of the associated MCV.

e. Upper-level features

Figure 12 shows the composite upper-level height field, as well as the horizontal divergence field at 200 hPa. It can be seen that there is a low-amplitude short-wave ridge centered near the MCV early on in the life cycle (Figs. 12a and 12b), shifting eastward at later stages (Figs. 12c and 12d). This ridge arises due to the strong upper-level mass source associated with the active convection of the parent MCS. The mass injected into the upper troposphere by the convection is then advected downstream by the relatively strong westerly flow at this level.

Associated with this upper-level ridge, there is a concentrated region of divergence just northeast of the vortex center (Fig. 12). This divergence maximum is collocated with a significant anticyclone at this level, which would be evident if the synoptic-scale height field were removed in Fig. 12. The divergence maximum corresponds to the upper-level outflow of the parent convection, arising due to a strong ageostrophic westerly jet streak that exits from the top of the convective system on its northeastern side (Fig. 13). This jet streak was an important component of the mature MCC composite of Maddox (1983; see his Fig. 5f); Fritsch and Maddox (1981) discuss the mechanisms for this jet streak. The upper-level divergence maximum tends to persist throughout the MCV life cycle, although it weakens significantly due to the frequent demise of strong convection near the MCV center. In some individual cases, this divergence maximum appears to reintensify when an MCV produces significant secondary convection.

f. Vertical structure

Figure 14 presents vertical profiles of the divergence and p velocity through the composite MCV center at the

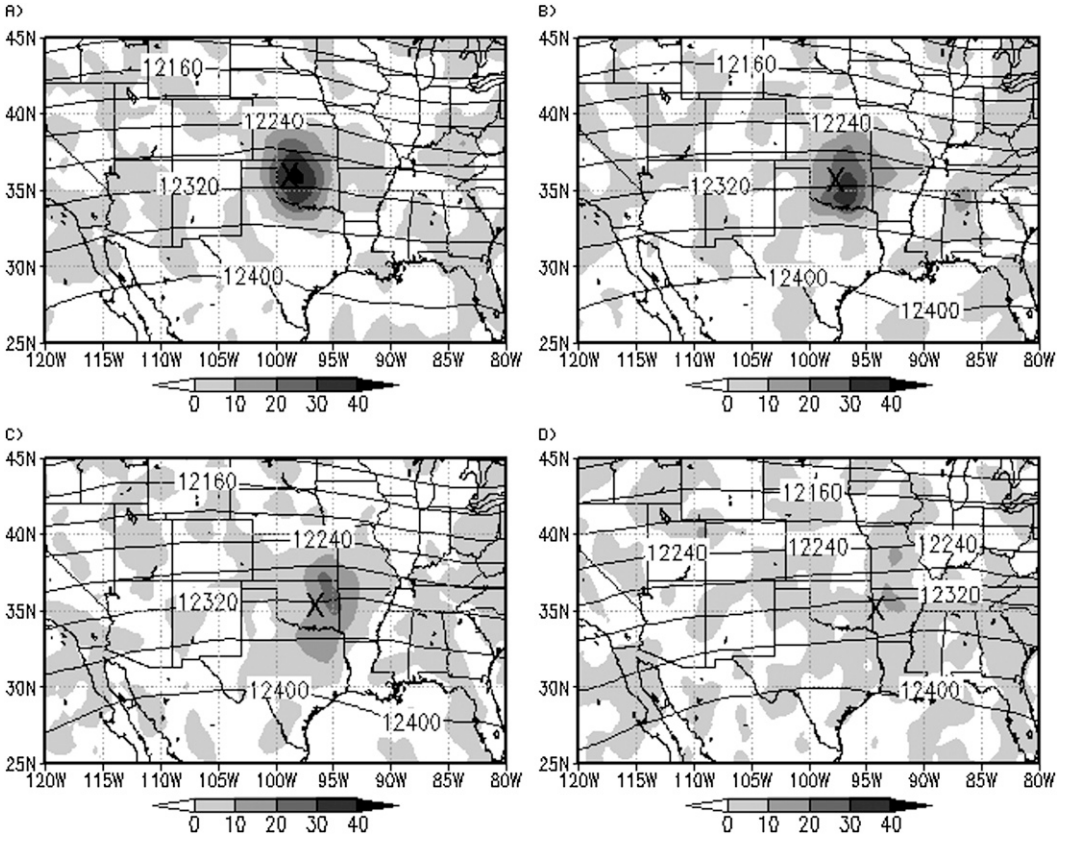

FIG. 12. RUC analyses of 200-hPa geopotential height (m; CI 40 m) and divergence (10^{-6} s^{-1}; shaded, with scale at bottom) at the (a) initiation, (b) development, (c) maturity, and (d) dissipation stages of the composite MCV. Composite vortex center is marked by a large cross in (a)–(d).

four life cycle stages. It should be noted that the pressure vertical velocity profile is taken directly from the RUC grid, rather than being derived from the divergence profile. The pressure vertical velocity variable is only available at the levels of 850, 700, 500, 300, and 200 hPa. The divergence profile (Fig. 14a) shows some significant variations during the MCV life cycle, most notably in the mid- and upper levels. At MCV initiation (light gray), at which time the convection associated with the parent MCS is most active, there is pronounced midlevel convergence and upper-level divergence. This differs from the ''before'' MCC composite divergence profile of Maddox (1983; see his Fig. 7); at MCC initiation, the environment tends to be characterized by strong convergence in the lower troposphere as deep, moist convection develops. At MCV initiation, however, the parent MCS has matured and developed widespread stratiform precipitation. The MCV initiation divergence profile seen in Fig. 14a, consisting of midlevel convergence, is characteristic of this stratiform precipitation (Mapes and Houze 1995). As expected from the conservation of mass, this divergence profile corresponds to strong mid- to upper-level ascent (Fig. 14b). This vertical motion profile resembles that determined by Gallus and Johnson (1992, their Fig. 4a) for the stratiform precipitation region during the early stage of an Oklahoma squall line. In later stages of the MCV life cycle, the midlevel convergence weakens and actually transitions into a divergence maximum by the dissipation stage. Over the same period, the upper-level divergence maximum gradually weakens (although it never transitions to convergence), and the mid- to upper-level ascent also weakens. In the lower troposphere, ascent occurs at the initiation stage due to active convection; this rising motion weakens at later stages as the convection dissipates and stratiform precipitation downdrafts become widespread. Increased low-level ascent at MCV dissipation may reflect the occasional resurgence of deep convection at this time.

Several previous studies (e.g., Fritsch et al. 1994; Davis and Trier 2002; Conzemius et al. 2007) have investigated individual MCVs from a potential vorticity (PV) perspective, presenting profiles and cross sections of PV from both observational and model data. The PV structure of the composite MCV constructed in this study

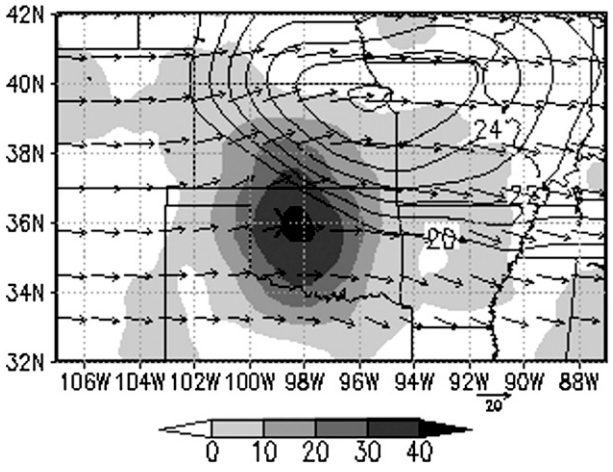

FIG. 13. RUC analysis of 200-hPa isotachs (m s^{-1}; CI 1 m s^{-1} above 20 m s^{-1}), wind vectors (20 m s^{-1} reference vector at bottom), and divergence (10^{-6} s^{-1}; shaded, with scale at bottom) at the initiation stage of the composite MCV. Composite vortex center is marked by a large cross.

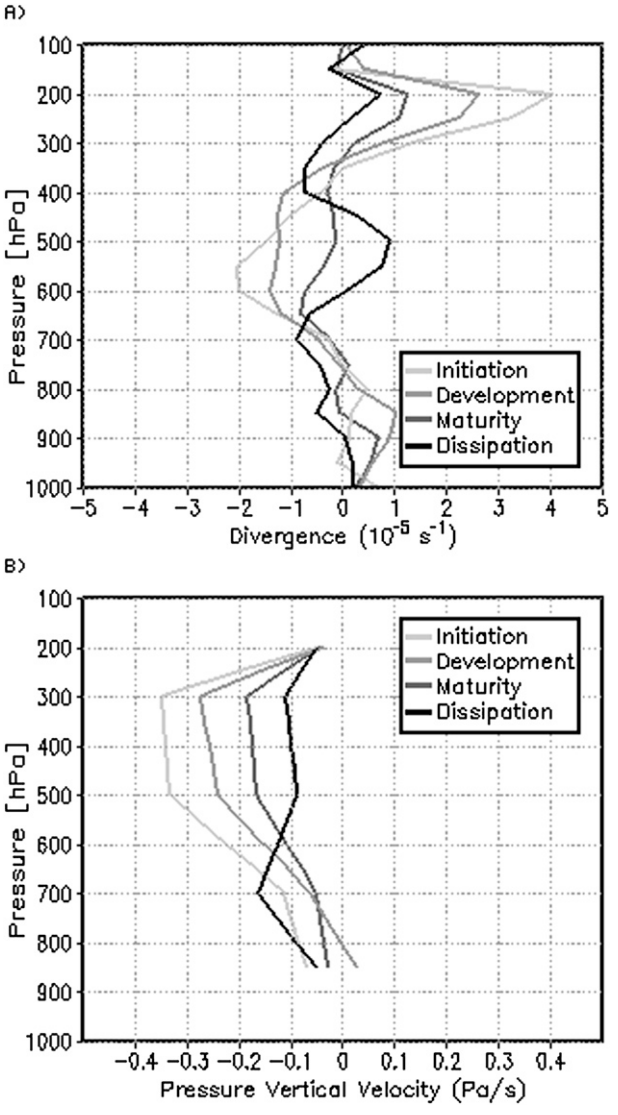

FIG. 14. RUC analyses of (a) divergence (10^{-5} s^{-1}) and (b) pressure vertical velocity (Pa s^{-1}) profiles through the composite MCV center at the initiation (light gray), development (medium gray), maturity (dark gray), and dissipation (black) stages of the composite MCV. Pressure vertical velocity is directly from the RUC, not calculated from the divergence profile. Pressure vertical velocity is only available at the pressure levels of 850, 700, 500, 300, and 200 hPa.

can be compared with these previous results. North–south cross sections through the center of the composite MCV at the four life cycle stages are shown in Fig. 15. The isentropes, contoured every 2 K, show the static stability component of the PV field. Also contoured is the potential temperature anomaly, displayed as the departure from the zonal mean within 5° longitude of the MCV. Note that the relevant thermal structure of the MCV is superimposed upon a synoptic-scale temperature gradient; the isentropes slope upward toward the north. At all four times, the MCV appears as a concentrated cyclonic PV anomaly with a maximum PV near or greater than 10^{-6} K m^2 kg^{-1} s^{-1} (1 PV unit; PVU) centered near 500 hPa. This anomaly occurs within a background 500-hPa PV of approximately 0.5 PVU. In the initiating composite (Fig. 15a), an elongated PV maximum appears at low levels (near 900 hPa). This maximum may be related to the presence of a low-level cold pool while the parent MCS is still active. It could also be due to enhanced low-level stability in the early morning hours, which tends to be the time of MCV initiation. A similar maximum was found by Fritsch et al. (1994) during their ''early development period'' (0600 UTC) for the MCV on 14–17 July 1982 (see their Fig. 24). This feature does not appear during the later stages of our MCV composite.

By the time of the developing composite (Fig. 15b), the MCV has intensified markedly. The isentropes within the PV maximum have become more closely spaced, indicating greater static stability. This greater stability is due to warming (depressed isentropes) immediately above the MCV and cooling (raised isentropes) immediately below the MCV. The mature MCV (Fig. 15c) shows a further intensification of the PV anomaly, with a relatively deep stable layer between 600 and 400 hPa, and a PV maximum of more than 1.25 PVU at 500 hPa. Cyclonic PV does extend downward somewhat toward the surface, but this extension remains relatively broad and weak in the composite. The positioning and magnitude of the PV maximum, as well as those of the distinct PV minimum above 300 hPa, agree well with the mature MCV cross section presented by Fritsch et al. (1994;

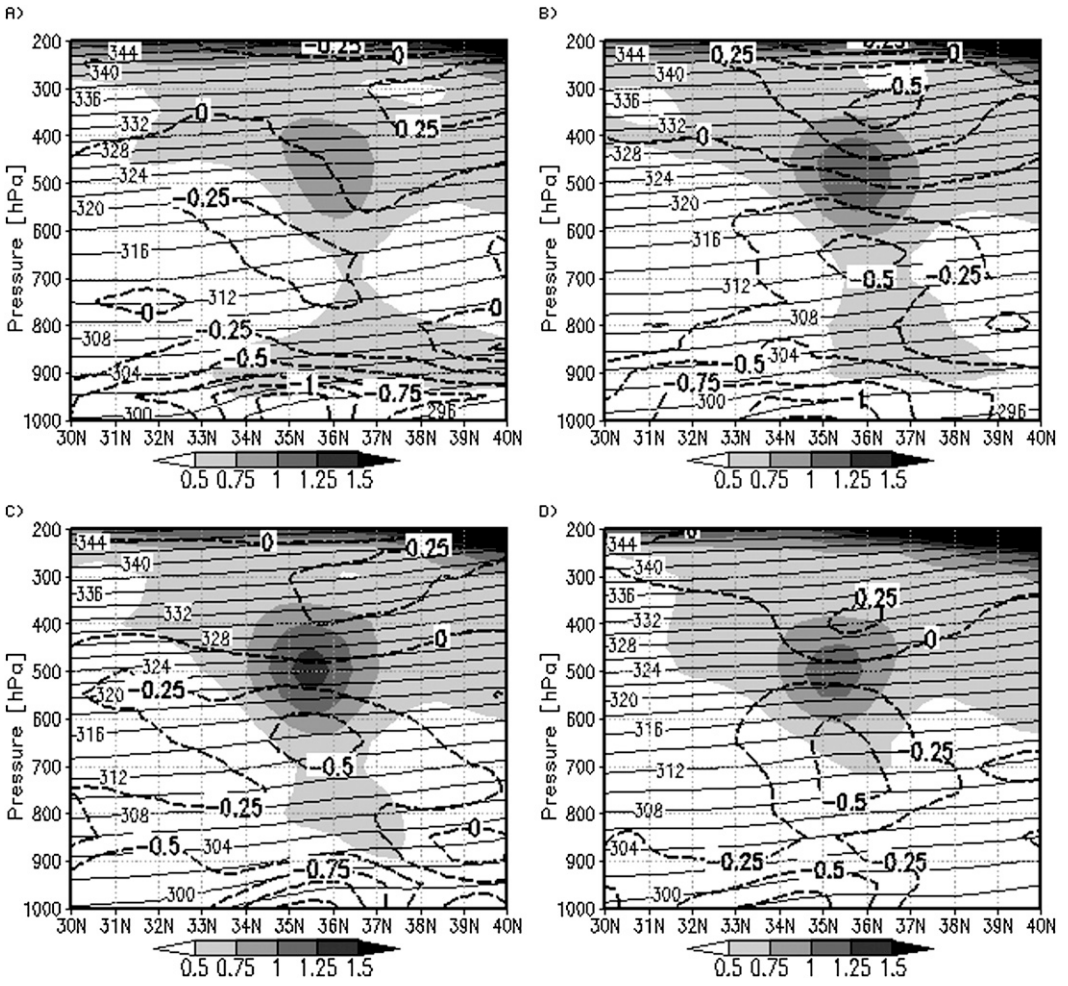

FIG. 15. RUC analyses of potential temperature (K; thin solid lines, CI 2 K), PV (10^{-6} K m^2 kg^{-1} s^{-1}; shaded, with scale at bottom), and potential temperature anomaly from the zonal mean (K; thick dashed lines, CI 0.25 K) along a north–south cross section at the (a) initiation, (b) development, (c) maturity, and (d) dissipation stages of the composite MCV.

see their Fig. 26). The dissipating composite (Fig. 15d) shows that the MCV has weakened by this time, although a midlevel PV maximum persists, together with the associated temperature perturbations.

Davis and Galarneau (2009) have hypothesized that some MCVs penetrate to the surface through the vertical coupling of a midlevel vortex and a convectively induced line-end vortex. The RUC dataset used to construct our composite is too coarse to resolve such a process, particularly considering the sparse observations in the vicinity of many of our MCVs.

g. Vertical wind shear

Previous research has stressed the importance of vertical wind shear within MCVs in determining vortex longevity (e.g., TDT) and the occurrence and location of MCV-induced secondary convection (e.g., Trier and Davis 2002). Therefore, in this section we investigate the vertical wind shear characteristics of our composite MCV. We use the wind profiles calculated as described in section 4a (an environmental wind profile at each life cycle stage for each MCV) to determine the composite wind profile at each life cycle stage. From this, following Trier and Davis (2007, hereafter TD), we calculate the wind shear over the 900–600-hPa layer. The vector difference in the winds between these two levels decreases from 8.9 m s^{-1} at the initiation stage to 6.3 m s^{-1} at the dissipation stage, from a direction of about 310°. Using standard atmosphere pressure–height conversions, these shear magnitudes correspond to 2.8 and 2.0×10^{-3} s^{-1}, respectively. These values are comparable with those of the composite of BM, although their calculations were over different pressure layers. Also consistent with their results, we observe a decrease in the environmental

wind shear during the MCV life cycle. Our shear values lie between the ''low level'' and ''midlevel'' values found by TDT.

To seek out a relationship between MCV longevity and environmental wind shear, we determine a mean environmental wind shear for each MCV case by averaging over the four MCV life cycle stages. Surprisingly, we find no significant relationship between MCV longevity and either the magnitude or direction of the 900–600-hPa wind shear. Past studies have suggested that such relationships may exist (e.g., TDT). It is possible that our result is due to the limitations of the RUC analyses; perhaps some long-lived MCVs in weak shear are not detected by our algorithm for as long as they actually exist.

TD present vertical profiles of several variables averaged over five MCV cases from the Bow Echo and MCV Experiment (BAMEX; Davis et al. 2004). They show profiles averaged over regions just upshear and downshear of the vortex center. Figure 16 displays similar profiles from our composite at MCV maturity. Following TD, we have determined the upshear and downshear directions for each case based on the 900–600-hPa wind shear direction. The composite upshear and downshear profiles for each variable are based on an average over a 1°-radius circle centered 2° upshear and downshear of each MCV center, respectively.

The average vertical profiles of divergence at MCV maturity are shown in Fig. 16a; this variable is not included by TD. While there are large differences between the divergence profiles of individual cases in our composite, interesting differences emerge between the upshear and downshear regions. Low- to midlevel convergence and upper-level divergence are more pronounced in the downshear profile (Fig. 16a). These profiles would lead to enhanced ascent downshear of the MCV, and reduced ascent upshear of the vortex. That this is the case is seen in Fig. 16b, which shows upshear and downshear profiles of the pressure vertical velocity (cf. with Fig. 9a of TD). Our pressure vertical velocity profiles are somewhat different from those of TD, partly due to the low vertical resolution of this variable in the RUC model. Also, unlike TD, we have not imposed a lower boundary condition of zero vertical velocity at the surface; instead, we display the raw model vertical velocities. Compared with TD, our profiles show generally smaller magnitudes of ascent in the downshear profile and more significant subsidence in the low to middle levels. Qualitatively, however, our results agree with those of TD in indicating a more favorable environment for convection downshear of the MCV.

Figure 16c shows profiles of potential temperature perturbations upshear and downshear of the MCV, and can be compared with Fig. 10a of TD (note that their figure only extends up to 600 hPa). The perturbations are calculated relative to the mean potential temperature profile over a 2°-radius circle centered on the MCV. In both figures, the potential temperature perturbations are essentially opposite in the upshear and downshear regions. However, the details of our profiles are quite different from those of TD, likely due to their limited sample size. The presence of a warm anomaly aloft and a cool anomaly at low levels in our downshear profile is consistent with the occurrence of precipitation systems downshear of the MCV. Such a temperature profile is suggested by the ''during'' MCC composite equivalent potential temperature profile shown by Maddox (1983, his Fig. 9c). The model fields should be viewed with caution in the lowest levels of the atmosphere, due to the elevated land surface.

Relative humidity profiles upshear and downshear of the MCV are presented in Fig. 16d. Remarkably, these profiles show very similar structure to the five-case average profiles of TD (their Fig. 11a). In the low levels, the upshear and downshear profiles are nearly identical, displaying a monotonic decrease with height. Relative humidity values are slightly higher in the BAMEX composite than in our composite. In the midtroposphere, however, both composites show a continued decrease in relative humidity with height in the upshear quadrant, but a significant increase with height in the downshear quadrant. It is possible that this increased midlevel relative humidity downshear of the vortex is due to the midlevel ascent in this region (Fig. 16b).

5. Summary and conclusions

This study has documented a number of climatological characteristics of midlatitude mesoscale convective vortices (MCVs) based on a fairly large sample of cases (45) observed over the state of Oklahoma during 4 yr (2002–05). MCV case detection was achieved with an objective algorithm developed to operate on analyses from the operational Rapid Update Cycle (RUC) model, as described by Davis et al. (2002). The use of this algorithm has allowed a meaningful comparison of the derived climatological aspects of our MCVs with the DAT study, and an extension of the DAT climatology to four additional years.

We have analyzed MCV cases during the months of May–August. To our knowledge, MCVs outside of this season in the United States have not been reported in the literature, although it is likely that they do sometimes occur. Our study period contains too many periods of missing RUC data to make any definitive statements about the seasonality of MCV occurrence within the

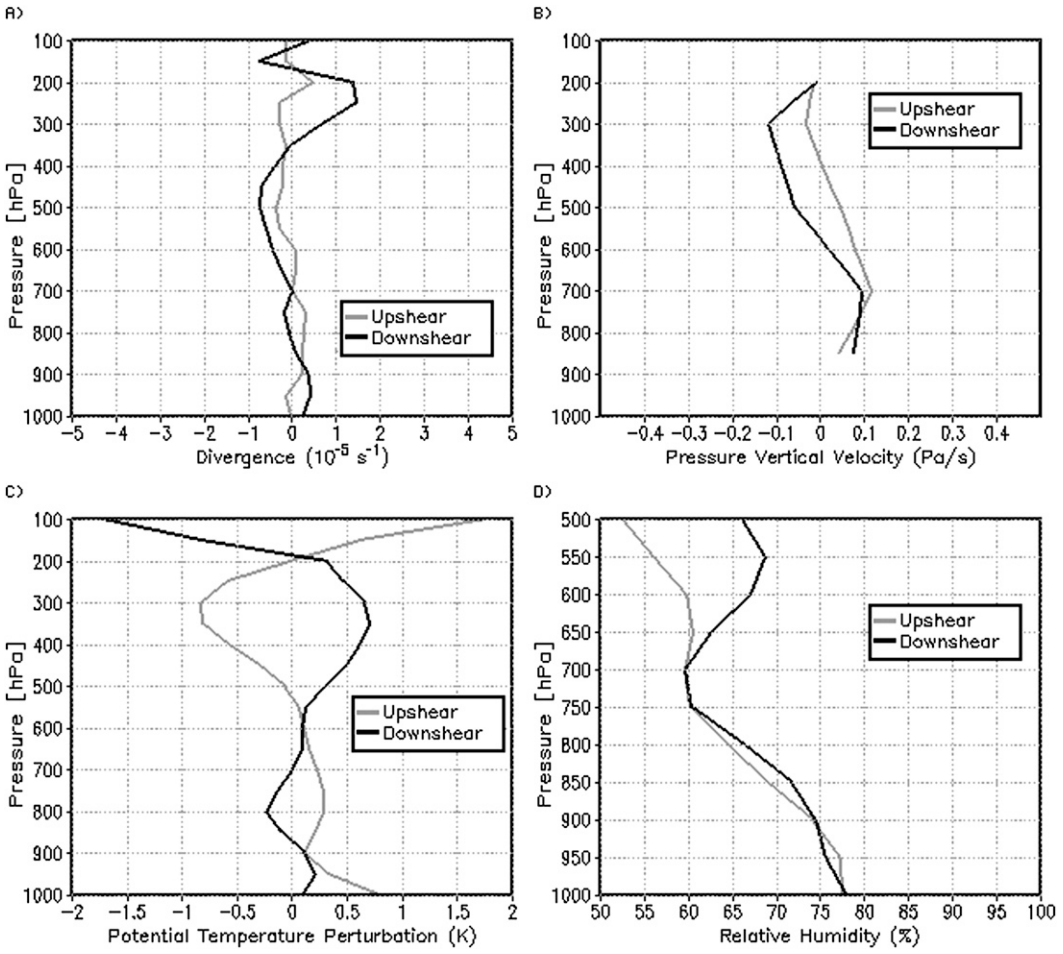

FIG. 16. RUC analyses of the (a) divergence (10^{-5} s^{-1}), (b) pressure vertical velocity (Pa s^{-1}), (c) potential temperature anomaly from zonal mean (K), and (d) relative humidity (%) profiles through regions immediately upshear (light gray) and downshear (black) of the composite vortex center at the maturity stage of the composite MCV. Pressure vertical velocity is directly from the RUC, not calculated from the divergence profile. Pressure vertical velocity is only available at the pressure levels of 850, 700, 500, 300, and 200 hPa.

convective season. Bartels and Maddox (1991) present the tracks of their MCV cases, and demonstrate that the main region of vortex activity shifts northward from May to July; our cases are limited to those occurring over Oklahoma, so we are unable to confirm this large-scale seasonal shift during 2002–05.

In agreement with DAT, it is found that true MCVs account for only about 20% of the midlevel mesoscale vortices occurring during the warm season over the Great Plains downstream of the Rocky Mountains. DAT have suggested that many of the other vortices may be topographically generated due to their concentration in the immediate lee of the Rocky Mountains. These ''dry vortices'' are also widespread in the southeastern United States (DAT) and in the domain delineated in this study. It is likely that other mechanisms, such as local instabilities of the mean flow, could produce such localized relative vorticity maxima in areas far away from significant topography.

It is found that MCVs have a typical radius of about 200 km, achieving their maximum relative vorticity (of about 10^{-4} s^{-1}) in the midtroposphere (from 600 to 500 hPa). The longevity of the MCVs varies widely, with some systems only detected for 1 h, and others lasting for more than 48 h. MCV longevity and intensity are found to be unrelated. Among the cases included here, we do not find a complete absence of weak, long-lived MCVs such as was found by DAT for their entire population of vortices. This could be due to our relaxation of DAT's requirement that an MCV must be nearly continuously detected by the objective algorithm in order to be considered a single MCV. This requirement likely led to a low bias in their MCV longevities, thus artificially removing weak, long-lived vortices from their sample.

The frequency of secondary convection (a second period of deep convective activity during the MCV life cycle) associated with the MCVs is found to be about 40%, similar to previous studies. MCVs with secondary convection last slightly longer, on average, than MCVs generating no secondary convection; this result is in qualitative agreement with theories regarding MCV intensification by secondary convection (e.g., Rogers and Fritsch 2001). However, part of this longevity difference may be due to the increased tendency for long-lived MCVs to trigger secondary convection.

We have presented the first relatively high-resolution composite analysis of the synoptic-scale environment of midlatitude MCVs. This analysis demonstrates that MCVs tend to initiate within mature, nocturnal mesoscale convective systems (MCSs; including mesoscale convective complexes). Features common to composites of both initiating MCVs and mature MCSs include an ageostrophic upper-level jet streak and associated divergence, midlevel convergence and ascent within the precipitation system, and a south-southwesterly low-level jet. MCS maturity and MCV initiation both tend to occur in the early morning hours; the initiation of the MCVs thus appears to be linked to the diurnal cycle. A mesoscale trough in the midlevel height field appears as the composite MCV intensifies and persists through MCV dissipation. Potential vorticity (PV) cross sections through the composite vortex confirm the general vertical structure documented in individual MCV cases studies. These cross sections reveal that the vortex circulation is, on average, confined to the midtroposphere, although there is some extension into the lower troposphere during the developing and mature stages. The development of a system-scale warm core is seen in the gradual depression of the mid- to upper-level isentropes within the cyclonic PV anomaly. Vertical profiles of several variables in the vicinity of the composite MCV reveal that the environment immediately downshear of the composite MCV is more conducive to the formation of secondary convection than the upshear environment.

While this work largely supports the conclusions of DAT regarding the frequency and characteristics of midlatitude MCVs, it also raises several important questions to be addressed by future research. It is unclear whether these results hold in other regions of the world where MCVs have been reported; it would be helpful if climatological studies of MCV populations were conducted in some of these regions, particularly very different ones such as the maritime tropics. It remains for future work to explore in more detail the nature of the relationship between MCV-induced secondary convection and the structural characteristics of the parent MCV. It would also be interesting to compare and contrast the climatological characteristics of the five independent midlatitude MCV types identified by James and Johnson (2010). Similarly, stratification of our MCV sample into MCVs with longevities greater than 10 h and less than 10 h reveals that there are significant differences in the composite structure and environment of these two subsets. Composite analyses of specific subsets of the total MCV population may reveal unique environmental features of some of these subsets, which would obviously be valuable for forecasting.

It is hoped that this climatology will be of use to operational forecasters, as well as serving as a basis for future research. Improvements in our understanding of the dynamics and evolution of MCVs will allow for progress in forecasting their associated hazards, including convective initiation, extreme rainfall, and tropical cyclogenesis.

Acknowledgments. RUC analyses were obtained from NOAA's National Operational Model Archive and Distribution System. The original MCV detection algorithm was provided by David Ahijevych of NCAR. We thank Russ Schumacher, Bob Conzemius, and an anonymous reviewer for very helpful comments that greatly improved the manuscript. This research was supported by National Science Foundation Grant ATM-0500061.

REFERENCES

Bartels, D. L., and R. A. Maddox, 1991: Midlevel cyclonic vortices generated by mesoscale convective systems. *Mon. Wea. Rev.,* **119,** 104–118.

Benjamin, S. G., and Coauthors, 2004: An hourly assimilation–forecast cycle: The RUC. *Mon. Wea. Rev.,* **132,** 495–518.

Bosart, L. F., and F. Sanders, 1981: The Johnstown flood of July 1977: A long-lived convective system. *J. Atmos. Sci.,* **38,** 1616–1642.

Carbone, R. E., J. D. Tuttle, D. A. Ahijevych, and S. B. Trier, 2002: Inferences of predictability associated with warm season precipitation episodes. *J. Atmos. Sci.,* **59,** 2033–2056.

Conzemius, R. J., R. W. Moore, M. T. Montgomery, and C. A. Davis, 2007: Mesoscale convective vortex formation in a weakly sheared moist neutral environment. *J. Atmos. Sci.,* **64,** 1443–1466.

Cotton, W. R., R. L. George, P. J. Wetzel, and R. L. McAnelly, 1983: A long-lived mesoscale convective complex. Part I: The mountain-generated component. *Mon. Wea. Rev.,* **111,** 1893–1918.

——, M.-S. Lin, R. L. McAnelly, and C. J. Tremback, 1989: A composite model of mesoscale convective complexes. *Mon. Wea. Rev.,* **117,** 765–783.

Davis, C. A., and S. B. Trier, 2002: Cloud-resolving simulations of mesoscale vortex intensification and its effect on a serial mesoscale convective system. *Mon. Wea. Rev.,* **130,** 2839–2858.

——, and T. J. Galarneau Jr., 2009: The vertical structure of mesoscale convective vortices. *J. Atmos. Sci.,* **66,** 686–704.

——, D. A. Ahijevych, and S. B. Trier, 2002: Detection and prediction of warm season midtropospheric vortices by the Rapid Update Cycle. *Mon. Wea. Rev.,* **130,** 24–42.

——, and Coauthors, 2004: The Bow Echo and MCV Experiment: Observations and opportunities. *Bull. Amer. Meteor. Soc.,* **85,** 1075–1093.

Fritsch, J. M., and R. A. Maddox, 1981: Convectively driven mesoscale weather systems aloft. Part I: Observations. *J. Appl. Meteor.,* **20,** 9–19.

——, J. D. Murphy, and J. S. Kain, 1994: Warm core vortex amplification over land. *J. Atmos. Sci.,* **51,** 1780–1807.

Gallus, W. A., Jr., and R. H. Johnson, 1992: The momentum budget of an intense midlatitude squall line. *J. Atmos. Sci.,* **49,** 422–450.

James, E. P., and R. H. Johnson, 2010: Patterns of precipitation and mesolow evolution in midlatitude mesoscale convective vortices. *Mon. Wea. Rev.,* **138,** 935–957.

Jiang, X., N.-C. Lau, I. M. Held, and J. J. Ploshay, 2007: Mechanisms of the Great Plains low-level jet as simulated in an AGCM. *J. Atmos. Sci.,* **64,** 532–547.

Keenan, T. D., and R. E. Carbone, 2008: Propagation and diurnal evolution of warm season cloudiness in the Australian and Maritime Continent region. *Mon. Wea. Rev.,* **136,** 973–994.

Laing, A. G., and J. M. Fritsch, 1993a: Mesoscale convective complexes in Africa. *Mon. Wea. Rev.,* **121,** 2254–2263.

——, and ——, 1993b: Mesoscale convective complexes over the Indian monsoon region. *J. Climate,* **6,** 911–919.

——, R. E. Carbone, V. Levizzani, and J. D. Tuttle, 2008: The propagation and diurnal cycles of deep convection in northern tropical Africa. *Quart. J. Roy. Meteor. Soc.,* **134,** 93–109.

Maddox, R. A., 1980: Mesoscale convective complexes. *Bull. Amer. Meteor. Soc.,* **61,** 1374–1387.

——, 1983: Large-scale meteorological conditions associated with midlatitude, mesoscale convective complexes. *Mon. Wea. Rev.,* **111,** 1475–1493.

Mapes, B. E., and R. A. Houze Jr., 1995: Diabatic divergence profiles in western Pacific mesoscale convective systems. *J. Atmos. Sci.,* **52,** 1807–1828.

Miller, D., and J. M. Fritsch, 1991: Mesoscale convective complexes in the western Pacific region. *Mon. Wea. Rev.,* **119,** 2978–2992.

Olsson, P. Q., and W. R. Cotton, 1997: Balanced and unbalanced circulations in a primitive equation simulation of a midlatitude MCC. Part I: The numerical simulation. *J. Atmos. Sci.,* **54,** 457–478.

Rogers, R. F., and J. M. Fritsch, 2001: Surface cyclogenesis from convectively driven amplification of midlevel mesoscale convective vortices. *Mon. Wea. Rev.,* **129,** 605–637.

Schumacher, R. S., and R. H. Johnson, 2008: Mesoscale processes contributing to extreme rainfall in a midlatitude warm-season flash flood. *Mon. Wea. Rev.,* **136,** 3964–3986.

——, and ——, 2009: Quasi-stationary, extreme-rain-producing convective systems associated with midlevel cyclonic circulations. *Wea. Forecasting,* **24,** 555–574.

Trier, S. B., and C. A. Davis, 2002: Influence of balanced motions on heavy precipitation within a long-lived convectively generated vortex. *Mon. Wea. Rev.,* **130,** 877–899.

——, and ——, 2007: Mesoscale convective vortices observed during BAMEX. Part II: Influences on secondary deep convection. *Mon. Wea. Rev.,* **135,** 2051–2075.

——, ——, and J. D. Tuttle, 2000: Long-lived mesoconvective vortices and their environment. Part I: Observations from the central United States during the 1998 warm season. *Mon. Wea. Rev.,* **128,** 3376–3395.

Velasco, I., and J. M. Fritsch, 1987: Mesoscale convective complexes in the Americas. *J. Geophys. Res.,* **92,** 9591–9613.

Wang, C.-C., G. T.-J. Chen, and R. E. Carbone, 2005: Variability of warm-season cloud episodes over East Asia based on GMS infrared brightness temperature observations. *Mon. Wea. Rev.,* **133,** 1478–1500.

Wetzel, P. J., W. R. Cotton, and R. L. McAnelly, 1983: A long-lived mesoscale convective complex. Part II: Evolution and structure of the mature complex. *Mon. Wea. Rev.,* **111,** 1919–1937.